J Mater Sci: Mater Electron (2023)34:548

Structural, transport, and thermoelectric properties of electron beam-irradiated $Bi_{1.2}Pb_{0.33}Sr_{1.54}Ca_{2.06}Co_3O_y$ cobalties

Sushmitha P. Rao[1], Ajay Kumar Saw[1], Chanderbhan Chotia[2], Vijay Pal Verma[3], V. C. Petwal[3], Jishnu Dwivedi[3], Gunadhor Okram[2], and Vijaylakshmi Dayal[1,*]

[1] Department of Physics, Maharaja Institute of Technology Mysore (Aff. VTU Belagavi), Mandya, Karnataka 571 477, India
[2] UGC DAE Consortium for Scientific Research, University Campus, Indore, MP 452001, India
[3] Industrial Accelerator Division, Raja Ramanna Centre for Advanced Technology, Indore, MP 452012, India

Received: 24 November 2022
Accepted: 19 January 2023

ABSTRACT

Electron beam (EB) irradiation has been extensively studied as a tool for tailoring the structural and electrical properties of a material. In this work, the influence of EB irradiation on the structural and transport properties of p-type thermoelectric $Bi_{1.2}Pb_{0.33}Sr_{1.54}Ca_{2.06}Co_3O_y$ misfit cobalties has been investigated. The EB doses range from 10 to 50 kGy. The X-ray diffraction patterns are analysed using Rietveld refinement, which revealed that pristine and irradiated samples possess a misfit-layered crystal structure composed of two monoclinic subsystems with different b-axis lengths. The EB irradiation caused the modification in lattice parameters, resulting in a moderate increase in misfitness (b_1/b_2) in the structures. Furthermore, the increase in EB irradiation dosages led to decreases in resistivity and an increase in the Seebeck coefficient, which can be attributed to the misfitness (b_1/b_2). The highest power factor is noted in the 50kGy EB-irradiated sample possessing a value of 284.51 $\mu W/mK^2$ at 224K and may be considered a promising material for thermoelectric device applications.

1 Introduction

The detrimental effect of utilizing non-renewable energy sources such as fossil fuels has driven the market for clean and green renewable energy sources. Thermoelectricity is a sustainable energy conversion method in which thermoelectric (TE) devices transform waste heat energy directly into electric power and vice versa. [1]. The thermoelectric material's performance is computed based on the parameter, known as the figure of merit 'ZT', mathematically given as, $(S^2/\rho K)T$ where S is the Seebeck coefficient, ρ is electrical resistivity, T is temperature, and K is thermal conductivity. In order to develop high-class

Address correspondence to E-mail: drvldayal@mitmysore.in; drvldayal@gmail.com

https://doi.org/10.1007/s10854-023-09926-2
Published online: 14 February 2023

material for the thermoelectric application, the *ZT* should be high. The challenge in enhancing this *ZT* stems from the inverse relationship between the aforementioned factors. [2]. Also, by raising the differential temperature amid the system's cold and hot ends, *ZT* can be improved under conditions where the system is allowed to run continuously at a high temperature in the air [3]. The intermetallic alloys and semiconductors such as $CoSb_3$ [4, 5] BiSb, Bi_2Te_3, and Sb_2Te_3 [6] have high *ZT* >1 and are most widely used. Recently, Bi_2Te_3 nanowire of width $N = 5$ has shown a high ZT of 2.5 at 350 K [7], and n-type SnSe possessed a high ZT of 2.8 ± 0.5 at 773 K [8]. Nonetheless, the detrimental nature and high cost of the aforementioned alloys make their practical applications challenging, and hence the study of silicides gained momentum. Silicides are earth-abundant and low-cost environmentally friendly materials with high $ZT > 2$ in n-type doped $Mg_2Si_{1-x}Sn_x$ [9]and $Si_{1-x}Ge_x$ [10], but their low melting point, as well as silicon's (Si) high thermal conductivity, created a pathway to the thermoelectric oxide materials [11]. In 1995, Slack et. al. anticipated that a good thermoelectric material would require a unique material property known as "Phonon-glass electron-crystal (PGEC)", which is a phenomenon of phonons scattering without significantly altering the electrical conductivity, comparable to its occurrence in glass-like materials [12]. In glass-like materials, the thermal conductivity is low due to the disordered exchange of energy within the domains and also possesses insulating behaviour in the absence of the desirable electron-crystal characteristics [13]. The cobalties are known to possess unique PGEC characteristics. Terasaki et al. initially in Na_xCoO_2 reported the highest *ZT* value of 0.26 at 300 K, understood due to its large Seebeck coefficient and low resistivity values [14]. Several studies have been conducted to understand the reasons for the coexistence of large thermopower and glass-like low thermal conduction along with the metal-like electrical conduction in cobalties [15–17]. One such explanation apprehended has been the misfitness (ranges from 1.6 to ~ 2) in the layered crystal structure [18]. Typically, the crystal structure of cobalties consists of two monoclinic layers: the insulating rock salt (RS) type block layer and the common conducting CdI_2 type CoO_2 octahedra of a two-dimensional triangular lattice [16]. This stacking of the layers of different symmetry leads to in-plane anisotropy in the cobalties and the lattice mismatch between these two layers causes chemical pressure along the b-axis [19]. Furthermore, considering the electronic structure, the Fermi energy (E_F) value in these cobalties has been characterized by a narrow band with a width of less than 2 eV, strong electron–electron correlation [17], and Kondo-like semiconductors behaviour [20]. Kondo semiconductors are expected to possess good thermoelectric characteristics with larger thermopower, as pointed out by Mahan et. al. [21]. Several misfits cobalt oxides with a layered structure such as $Ca_3Co_4O_9(Co-349)$ [22, 23], $Bi_2Sr_2Co_2O_y(BC-222)$ [23] and $Bi_2Sr_2CaCo_2O_{8-\delta}(Bi-2212)$ [24, 25] have been studied to improve the thermoelectric properties of the rock-salt substructure, and several approaches have been adopted to change the ratio of misfitness (b1/b2) or oxidation states of cations. [19, 26, 27]. Furthermore, adopting quite a few like, physical, chemical, and/or mechanical methods, cobalties show strong crystallographic anisotropy behaviour by developing plate-like grains, a shape anisotropy characteristic. This anisotropy allows grains of conducting planes to align preferentially, enabling the material to possess high electrical conductivity [28]. To further improve the material's functionality, several post-synthesis processes have also been undertaken, such as subjecting the materials to extremely intense radiations, like electron beams (EB), gamma rays, ion beams, and neutron beams. The aforementioned high-energy particles interact with materials causing defects like vacancies, interstices, and ionization. [29–32]. Kim et. al. reported a 5% enhancement in the power factor in the electron beam-irradiated $Si_{1-x}Ge_x$ thin film [13]. Sotelo et. al. reported that substituting Pb^{2+} to the Bi^{3+} site is one of the effective ways to induce cation in the rock salt sub-structure and enhance thermopower [3]. Keshri et. al. reported non-stoichiometric $Bi_{1.2}Pb_{0.33}Sr_{1.54}Ca_{2.06}Cu_3O_y$, which is poorer in Bi and Sr concerning 2 : 2 : 2 : 3 and substituted of Pb^{2+} to Bi^{3+} site to form stable compound synthesized under normal condition [33]. In this study, in accordance with the aforediscussed Bi-based cobalties, we have synthesized a non-stoichiometric $[(Bi,Pb)_{1.5}(Sr,Ca)_{3.5}O_y]_xCoO_2$ where ($x = 1.02$) via nitrate route. In order to enhance the thermoelectric performances, the ratio of misfitness (b_1/b_2) has been altered by subjecting the synthesized $Bi_{1.2}Pb_{0.33}Sr_{1.54}Ca_{2.06}Co_3O_y$ to EB irradiation.

2 Experimental

Polycrystalline samples of $Bi_{1.2}Pb_{0.33}Sr_{1.54}Ca_{2.06}Co_3O_y$ was synthesized using the nitrate method. The dilute nitric acid solution was used to dissolve the stoichiometric amounts of bismuth oxide (Bi_2O_3), lead (II) nitrate, $[Pb(NO_3)_2]$, strontium carbonate ($SrCO_3$), calcium carbonate ($CaCO_3$), and cobalt acetate $(CH_3COO)_2Co$. The gel was dried at 400 °C for 4 h, calcined for 8h at 600 °C, and finally sintered at 800 °C for 48 h with intermediate grindings and pelletization. To confirm phase purity and formation, a Bruker D8 Advance X-ray diffractometer was used to acquire a powder X-ray diffraction ($CuK\alpha$radiation) pattern. The elemental and morphological analysis was carried out using energy-dispersive X-ray (EDS) and scanning electron microscope (SEM). Raman measurements were taken using the 488 nm (2.53 eV) LabRAM – HR800 spectrometer. The thermopower measurement was taken using an automated precision load-based measurement setup in the temperature range of 10–300 K, inbuilt at UGC-DAE Consortium for Scientific Research, Indore [34, 35], and the resistivity measurement was taken using a standard four-probe technique using a homemade resistivity insert.

3 Results and discussion

3.1 X-ray diffraction study and SEM analysis:

The room temperature (RT) powder X-ray diffraction (XRD) patterns of pristine and irradiated $Bi_{1.2}Pb_{0.33}Sr_{1.54}Ca_{2.06}Co_3O_y$ samples, along with the Rietveld pattern [36] refined using FullProf software [37] are shown in Fig. 1

The samples are seen to be indexed into two monoclinic subsystems of a layered cobalt crystal with common axes of $[100]^*$ and $[001]^*$ and a misfit parameter of $[010]^*$ [38, 39]. Furthermore, the CoO_2 and RS $(Bi,Pb)_{1.5}(Sr,Ca)_{3.5}O_y$, are two-layered structural phases that are alternately arranged along the c-axis. Each Co atom in the CoO_2 layer is surrounded by six O atoms in an edge-sharing octahedral shape and the four consecutive layers of Sr(Ca)O–Bi(Pb)O–Bi(Pb)O–Sr(Ca)O surround the RS layer. It has been observed that the lattice properties of the irradiated samples change fairly without changing the crystal structure. Irradiation causes a rise in (b1/b2), which causes defects to occur owing to vacancy. The key aspect influencing the electrical properties of misfit cobalties is an increase in the misfitness ratio (b1/b2) with increasing EB irradiation dosage. The structural parameter values obtained from the refinement are listed in Table 1.

As discussed earlier, EB irradiation induces internal strain in the crystal structure by creating lattice distortions. To confirm the intrinsic strain and to calculate the average crystallite size of pristine and irradiated samples Williamson and Hall (W–H) equation has been adopted [40–42] (Eq. 1).

$$\beta \cos \theta = \frac{K\lambda}{D} + 4\varepsilon \sin \theta \tag{1}$$

Here β = full width half maximum (FWHM), θ = diffracting angle, K = Scherrer constant (0.9), $\lambda = 1.5406A^0$(Wavelength of $CuK\alpha$), D = crystalline size and, ε is the strain [40]. As illustrated in Fig. 2, the plot is drawn with $\beta\cos\theta$ along the y-axis and $4\sin\theta$ along the x-axis. The lattice strain and crystalline size are estimated from the slope and the

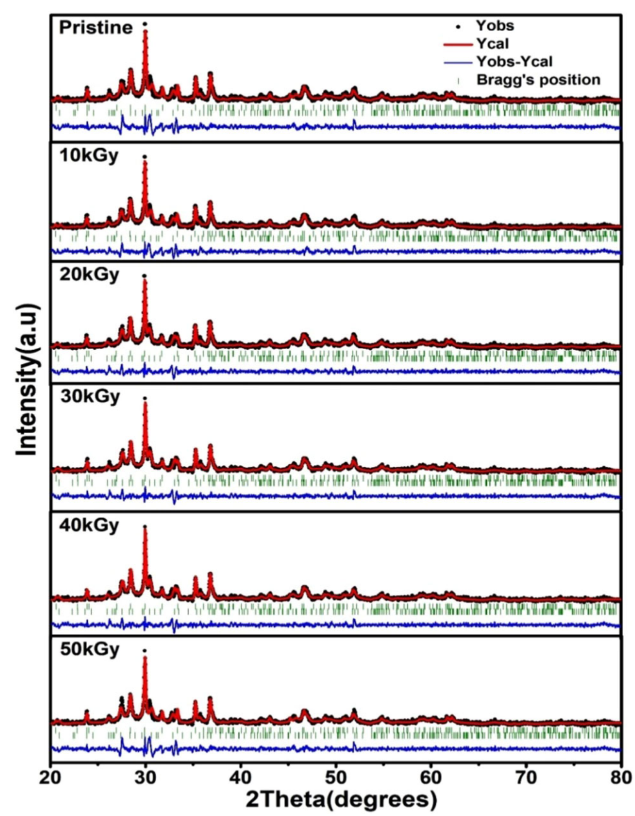

Fig. 1 Rietveld refinement of pristine and EB-irradiated $Bi_{1.2}Pb_{0.33}Sr_{1.54}Ca_{2.06}Co_3O_y$

Table 1 Structural parameters obtained by Rietveld analysis of the XRD pattern:

Parameters/samples	Pristine	10 kGy	20 kGy	30 kGy	40 kGy	50 kGy
Crystal structure	Monoclinic	Monoclinic	Monoclinic	Monoclinic	Monoclinic	Monoclinic
Space group	pm	pm	pm	pm	pm	pm
a1 = a2(A°)	4.749(5)	4.808(2)	4.913(8)	4.907(9)	4.822(2)	4.593(8)
b1(A°)	4.351(5)	4.258(3)	4.386(8)	4.385(6)	4.750(3)	4.674(4)
b2(A°)	2.778(3)	2.701(9)	2.694(2)	2.688(7)	2.704(5)	2.582(2)
c1 = c2(A°)	14.812(1)	14.994(7)	14.574(2)	14.577(5)	14.969(8)	14.915(7)
β1 = β2 (degrees)	95.230(5)	97.221(5)	96.178(5)	96.303(5)	95.276(1)	94.821(5)
b1/b2	1.566(2)	1.576(1)	1.628(2)	1.631(1)	1.756(4)	1.810(5)
Rp	1.32(4)	2.89(3)	3.30(8)	3.22(5)	2.02(7)	0.89(9)
χ^2	2.43	1.90	1.50	1.53	1.28	1.63
Crystalline size (nm)	22.34	22.45	22.59	22.66	22.87	22.91
Strain (10^{-3})	9.11	9.12	9.55	9.94	10.13	11.23

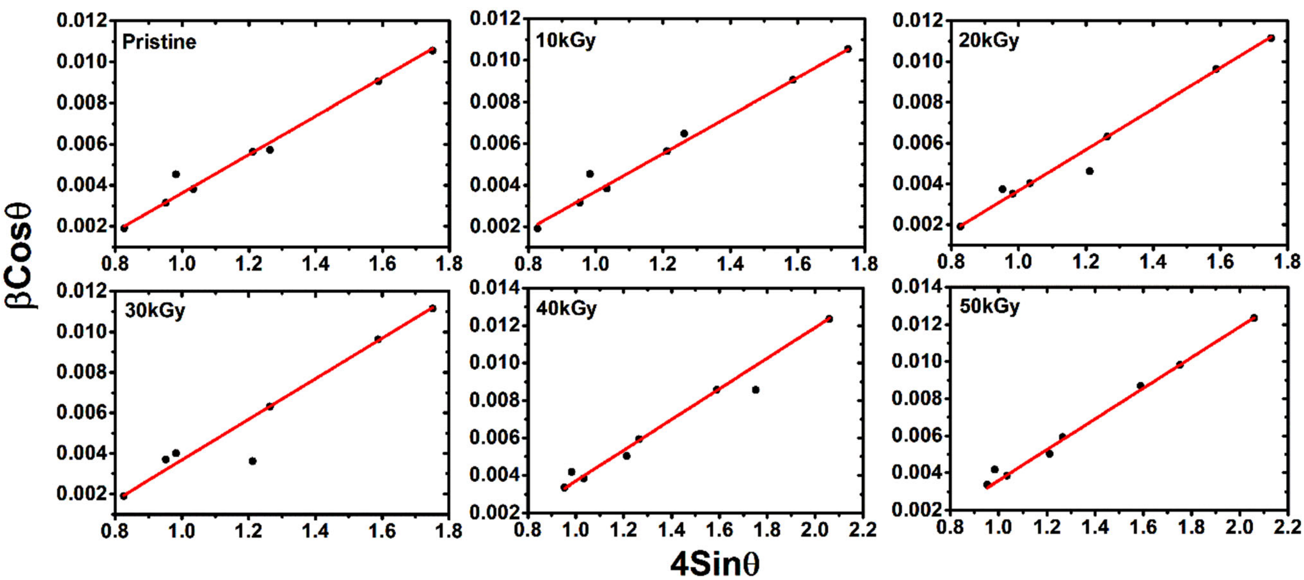

Fig. 2 Plot of $\beta_{hkl}Cos\theta$ V/s $4Sin\theta$ of pristine and EB-irradiated $Bi_{1.2}Pb_{0.33}Sr_{1.54}Ca_{2.06}Co_3O_y$

intercept of the plot and are tabulated in Table 1. The crystalline size has been observed to grow with the increase in EB dosage. This increase in crystalline size caused by EB irradiation can be attributed to a rise in crystal order caused by enabling grains to orient in a preferable direction [43]. The increased strain values with increasing EB irradiation, confirm that the EB irradiation induces strain in the crystal structure, which may result in an increase in misfit along the b-axis.

Figure 3 shows the SEM images of pristine and EB-irradiated $Bi_{1.2}Pb_{0.33}Sr_{1.54}Ca_{2.06}Co_3O_y$. The morphology of the samples suggests that the pristine and EB-irradiated samples have randomly oriented flat grains of similar size which are densely distributed. Kudo et. al. reported that EB irradiation increases the order of the crystal [44]. Takashiri et al. observed that EB irradiation causes atoms in the crystal to migrate, resulting in the seed crystal orienting in the favoured direction [43]. In this study, in the SEM images of 10 – 30kGy, any observable change has not been observed compared to pristine sample images. As mentioned earlier the grains of conducting planes can be preferentially oriented using physical, chemical, and/or mechanical processes [28]. In 40 and 50kGy-irradiated samples, an increment in grain size has been observed, which suggests that EB irradiation alters surface and cross-sectional morphology [45]. This has been verified by calculating the average grain size using Image-J software, which is shown as

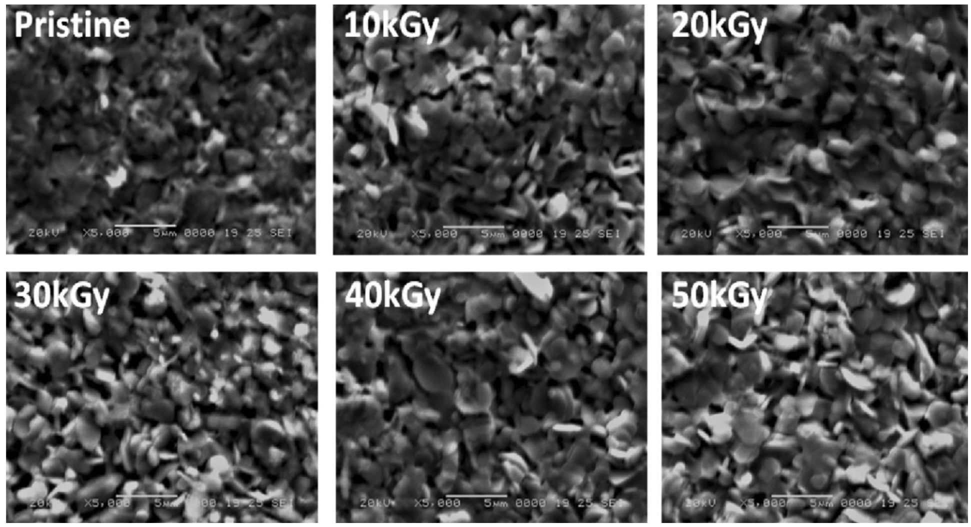

Fig. 3 SEM images of pristine and EB-irradiated $Bi_{1.2}Pb_{0.33}Sr_{1.54}Ca_{2.06}Co_3O_y$

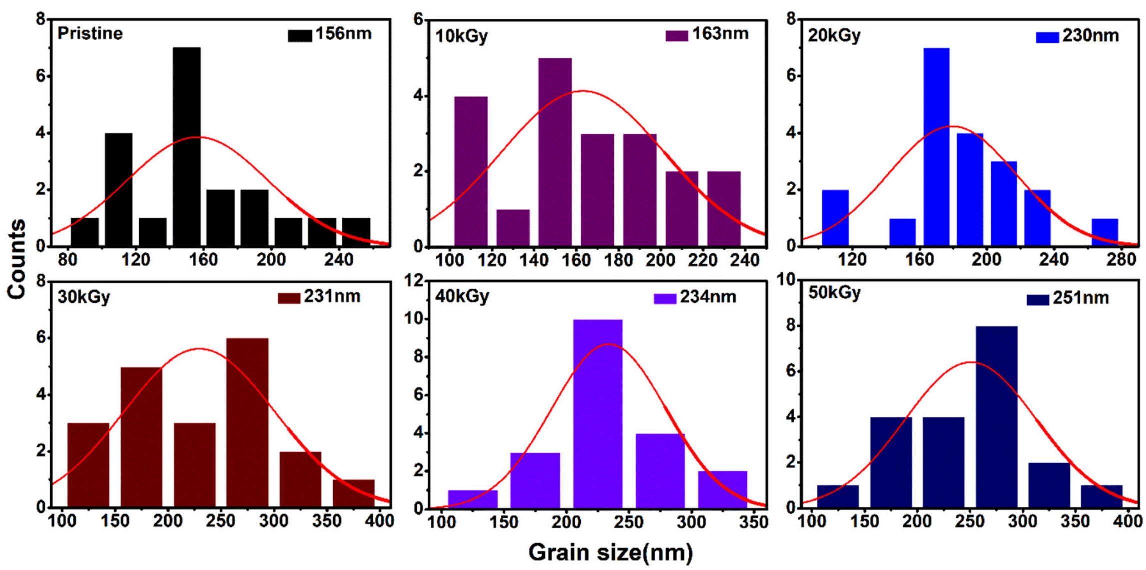

Fig. 4 Histogram indicating grain size of pristine and EB-irradiated $Bi_{1.2}Pb_{0.33}Sr_{1.54}Ca_{2.06}Co_3O_y$

a histogram plot in Fig. 4. It has been found that the grain size increased with the increase in EB irradiation dosage. The stoichiometric compositions were determined using EDS. The EDS mapping of the pristine and 50kGy EB-irradiated sample is shown in Fig. 5, which reveals that the stoichiometric composition remains intact during sample preparation and after the EB irradiation.

Raman spectroscopy is used to analyse the lattice structure, distortions in the crystal, ion distribution, etc. Figure 6 shows the RT Raman spectra of the pristine and EB-irradiated $Bi_{1.2}Pb_{0.33}Sr_{1.54}Ca_{2.06}Co_3O_y$ recorded in the wavelength range of $150-780cm^{-1}$.

For the pristine and EB-irradiated samples, the four phonon peaks were observed at $219cm^{-1}$ (P1), $290cm^{-1}$ (P2), $452cm^{-1}$ (P3), and $615cm^{-1}$ (P4). By the approximation of a harmonic oscillator, $w = \left(\frac{k}{\mu}\right)^{\frac{1}{2}}$, where '*k*' and 'μ' are force constant and reduced mass, respectively, the heavier atoms must vibrate in the low wave number zone [46]. Here, the vibrations significant to heavier atoms like Bi, Sr, Ca, Co, etc., would be lower than $150cm^{-1}$ and higher for lighter O atoms [47]. Therefore, we understand that peaks P1, P2, P3, and P4 resemble the vibration of oxygen atoms. The vibrations of O atoms in the $Co-O$ and $Ca-O$ planes of the Ca_2CoO_3 layers, respectively, can

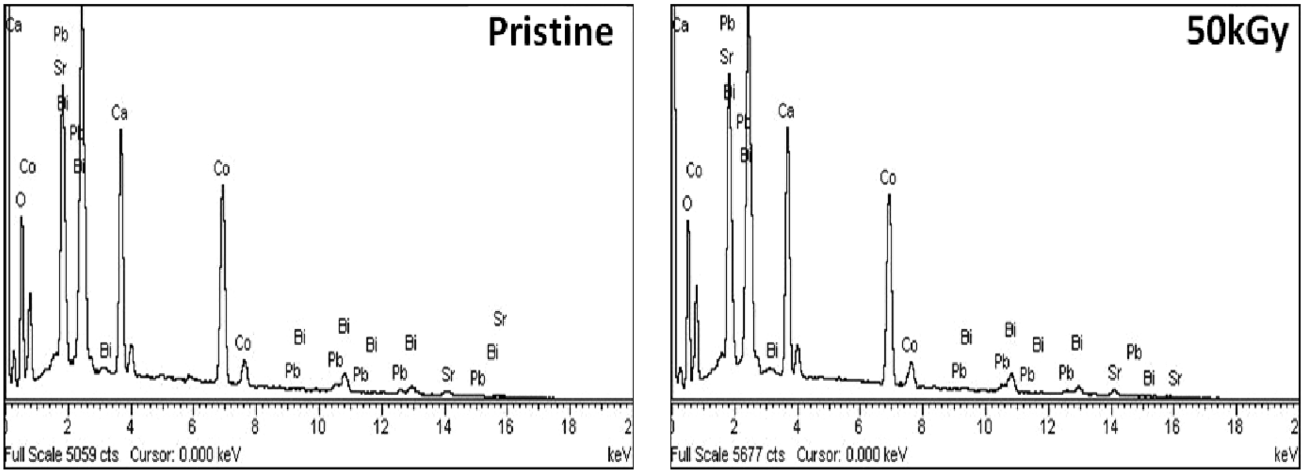

Fig. 5 EDS plot of pristine and 50 kGy EB-irradiated $Bi_{1.2}Pb_{0.33}Sr_{1.54}Ca_{2.06}Co_3O_y$

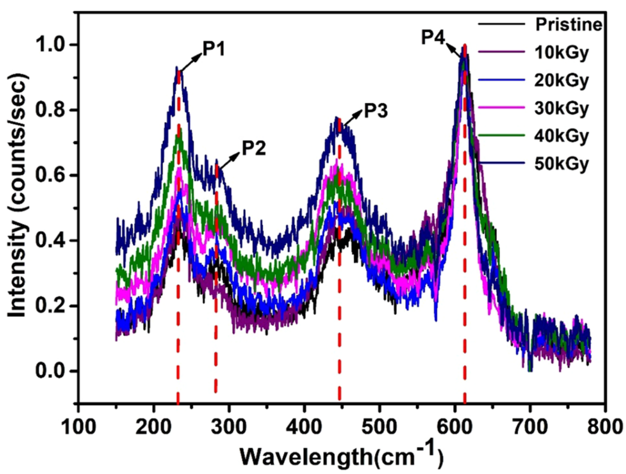

Fig. 6 Room temperature Raman spectra of pristine and EB-irradiated $Bi_{1.2}Pb_{0.33}Sr_{1.54}Ca_{2.06}Co_3O_y$

be connected to P1 and P2 [48, 49]. It is reasonable to assign P1 and P2 to the F_{2g} phonon [50]. P3 and P4 to E_{1g} and A_{1g} phonon compared with E_{1g} phonon with 472 cm^{-1} and A_{1g} phonon with 593 cm^{-1} for Na_x-CoO_2 [51]. The intensity of Raman spectra increases with increasing EB irradiation which confirms the increased defect density upon EB irradiation [52].

3.2 Electrical and thermoelectric properties

Figure 7a shows the temperature (T)—dependent resistivity (ρ) plot of pristine and electron beam-irradiated $Bi_{1.2}Pb_{0.33}Sr_{1.54}Ca_{2.06}Co_3O_y$. The resistivity increased with a decrease in temperature suggesting the insulating behaviour of studied samples measured in the temperature range 10–300K. Furthermore, the resistivity value is seen to decrease with an increase in EB irradiation. This decrease in resistivity

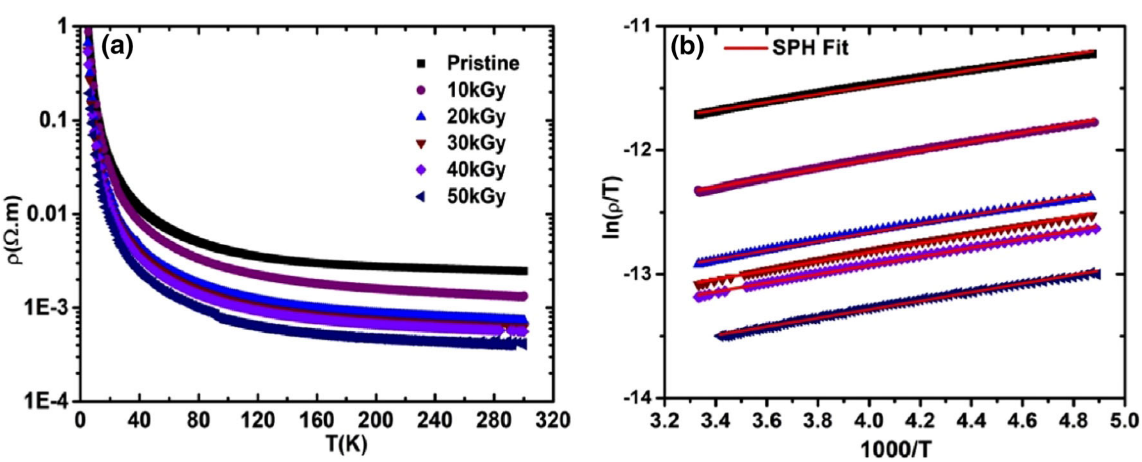

Fig. 7 **a** Temperature (T)-dependent resistivity (ρ) plot, **b** fitting of (ρ) of pristine and EB-irradiated $Bi_{1.2}Pb_{0.33}Sr_{1.54}Ca_{2.06}Co_3O_y$

can be attributed to lattice strain and possibly due to the creation of holes via defects due to the bombardment of EB. Since the studied samples are p-type, the creation of holes via defects enhances carrier concentration (p). The resistivity equation, i.e., $\rho = {}^{1}/_{pe\mu}$, where 'p' is the carrier concentration of holes, 'e' is the charge of an electron, and 'μ' is the mobility, suggesting that the resistivity varies inversely with carrier concentration. Thus the decrease in resistivity due to the bombardment of EB is evident due to increase in p-type carriers. The decrease of resistivity with EB irradiation has also been reported in $Pr_{0.8}Sr_{0.2}CoO_3$ cobalties by Christopher et. al.[53].

It is also widely known that in cobalties tiny polarons are typically produced by the excitation of electrons from the constrained band of the low spin state of the 'e_g' orbital to the excited state of $Co - 3d$ [54]. The resistivity data were examined by taking the small polaron hopping (SPH) model [55] mentioned in Eq. 2 to understand the transport mechanism of temperature-dependent resistivity of pristine and EB-irradiated materials.

$$\rho(T) = \rho_\alpha T.exp\frac{E_A}{k_B T} \qquad (2)$$

In this equation, 'E_A' = activation energy and 'K_B' = Boltzmann constant, $\rho_\alpha = \frac{2K_B}{3pe^2a^2\vartheta}$ represents the coefficient of resistivity, 'e' electron charge, 'a' site to site hopping distance and 'ϑ' is longitudinal optical phonon frequency. The resistivity data in the high-temperature regime has been studied using Eq. 2, and accordingly the plot of $\ln(\rho/T)$ vs temperature inverse $(1/T)$ for pristine and electron beam-irradiated $Bi_{1.2}Pb_{0.33}Sr_{1.54}Ca_{2.06}Co_3O_y$ is shown in Fig. 7b. The good fitting of the resistivity data to Eq. 2 implies that tiny polarons are responsible for conduction at high temperatures. Table 2 displays the relevant parameter's best-fit value. One can note that an increase in EB irradiation dosage increased the activation energy (E_A) while lowering the ρ_α, signifying the presence of weak double exchange (DE) [45, 56]. It is well-accepted that the coefficient of resistivity (ρ_α) is inversely proportional to site-to-site hopping distance 'a', thus hopping energy increases with irradiation, which also caused a decrease in electrical resistivity [54, 57].

The temperature-dependent Seebeck coefficient *(S)* of pristine and electron beam-irradiated $Bi_{1.2}Pb_{0.33}Sr_{1.54}Ca_{2.06}Co_3O_y$ is shown in Fig. 8a in the temperature range (10–300K). $S = \Delta V/\Delta T$ where ΔV is the thermoelectric potential difference, and ΔT is the temperature difference between the hot and cold end. The studied samples are purely p-type at par with the reported cobalties, and the positive S value in the measured temperature range shows that the holes are the predominant charge carriers [3]. The Seebeck coefficient makes it clear that the Jahn Teller (JT) distortion predominates in the samples, as when sufficiently strong static JT distortions are present, holes are the predominant charge carriers [54].

Furthermore, the metal-to-insulator transition at characteristic temperatures, 'Ts' is noticeable in the studied samples and can be attributed to confined charge carriers controlled by polarons causing the metal-to-insulator transition. One can note the Seebeck coefficient value increases as the EB irradiation dosage is increased, which can be ascribed to the lattice defects, specifically vacancy, created due to EB

Table 2 Fitting parameters calculated from resistivity and thermopower data of pristine and EB-irradiated $Bi_{1.2}Pb_{0.33}Sr_{1.54}Ca_{2.06}Co_3O_y$ samples

Parameters/sample	Pristine	10 kGy	20 kGy	30 kGy	40 kGy	50 kGy
E_A (meV)	27.78 ± 0.82	29.84 ± 0.76	30.56 ± 0.91	30.96 ± 0.78	31.24 ± 0.94	31.54 ± 0.89
ρ_α (Ωm)(10^{-3})	− 14.66 ± 2.01	− 14.34 ± 2.03	− 14.27 ± 2.27	− 14.10 ± 2.53	− 13.54 ± 2.41	− 12.77 ± 2.21
S_o (μV/K)	61.89 ± 1.65	74.35 ± 1.41	50.01 ± 0.78	39.65 ± 1.29	48.24 ± 2.07	6.42 ± 0.84
$S_{3/2}$(μV/$K^{1.5}$)	− 2.86 ± 0.24	− 8.09 ± 0.76	− 8.59 ± 0.53	− 8.80 ± 0.77	− 8.85 ± 0.97	− 10.12 ± 0.84
S_2(μV/K^2) (10^{-2})	1.60 ± 0.06	0.05 ± 0.06	1.39 ± 0.05	0.56 ± 0.06	0.63 ± 0.10	1.06 ± 0.04
S_3(μV/K^3)	1.43 ± 0.25	4.30 ± 0.64	4.04 ± 0.49	4.43 ± 0.42	4.40 ± 0.11	5.06 ± 0.54
S_4(μV/K^4) (10^{-8})	− 19.24 ± 1.27	− 15.86 ± 1.63	− 6.52 ± 1.42	− 12.94 ± 1.61	− 15.55 ± 2.75	− 24.67 ± 1.09
E_S (meV)	1.12 ± 0.21	1.63 ± 0.04	2.01 ± 0.17	2.02 ± 0.01	2.84 ± 0.14	2.94 ± 0.05
α	− 1.19 ± 0.08	− 1.12 ± 0.04	− 1.03 ± 0.03	− 1.02 ± 0.03	− 0.75 ± 0.04	− 0.84 ± 0.01
T_s (K)	192.64	210.09	183.29	226.87	219.69	214.11

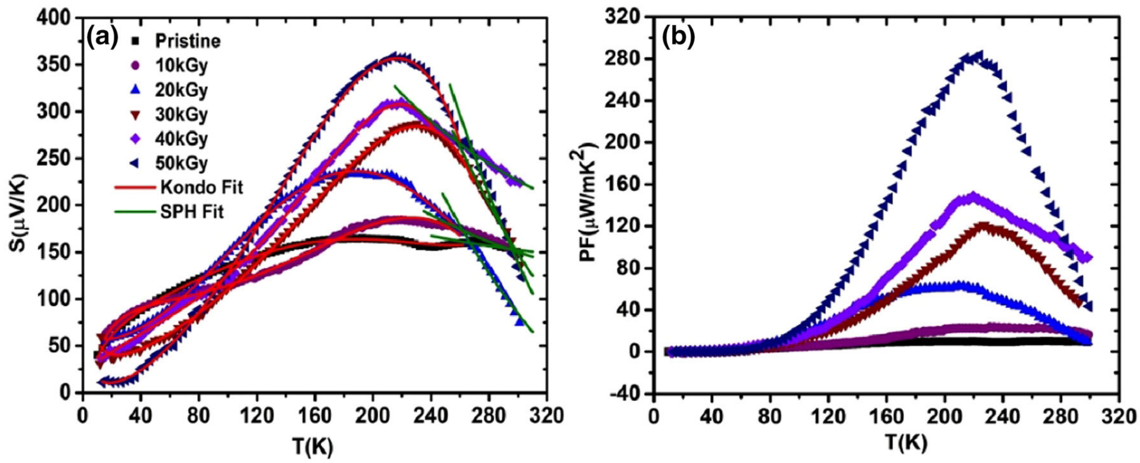

Fig. 8 **a** Temperature (*T*)-dependent Seebeck coefficient (S) with the fitting of (S) **b** Power factor of pristine and EB irradiated $Bi_{1.2}Pb_{0.33}Sr_{1.54}Ca_{2.06}Co_3O_y$

irradiation. According to Fujii et al., the mismatch between the CdI2type and rock salt layers causes a significant anisotropic Seebeck coefficient in cobalties [38]. From Table 1, it is evident that the increase in EB dosage increases the ratio of misfitness, thereby increasing the Seebeck coefficient. The highest observed Seebeck coefficient, 358.53μV/K is observed for the 50kGy EB irradiated sample.

The Seebeck coefficient has been examined using Eq. 3 to understand the contributions of the various scattering mechanism in the metallic region of the studied samples.

$$S(T) = S_0 + S^{3/2}T^2 + S_4T^4 \tag{3}$$

where S_0 has no physical origin, $S^{3/2}T^2$ contributed by electron–magnon scattering, and S_4T^4 contributed by spin-wave fluctuations [58, 59]. The experimental data were initially fitted with Eq. (3) and it can be observed that Eq. (3) is insufficient to fit and explain the conduction mechanism. As discussed earlier the cobalties belong to the special class of material called Kondo semiconductors and the evident slight upturn trend in the low-temperature region in the Seebeck coefficient plot suggests Kondo-like scattering in the studied samples. Therefore, it is plausible to add the Kondo term in Eq. (3) and the modified equation is given by;

$$S(T) = S_0 + S_{3/2}{}^{3/2}T^2 + S_2T^2 + S_3T^3 + S_4T^4 \tag{4}$$

where S_2T^2 is due to kondo-like scattering and S_3T^3 is due to phonon drag produced by electron–phonon interaction. The best-fit values are tabulated in Table 2. The best-fit scattering coefficient values confirm that EB irradiation creates a vacancy, which enhances scattering and results in a higher Seebeck coefficient.

The high-temperature insulating regime of $S(T)$ is fitted by Mott's polaron hopping model [32] using Eq. 5.

$$S(T) = \frac{K_B}{e}\left[\frac{E_S}{K_BT} + \alpha\right] \tag{5}$$

Here, 'E_S' is the activation energy, and 'α' is the constant governing the relationship between heat transfer and an electron's kinetic energy. If $\alpha < 1$ indicates a small polaron exists, whereas ($\alpha > 1$) implies the existence of large polarons. It is observed that the activation energy 'E_S' increases with an increase in EB irradiation dose. A similar trend of 'E_A' has been observed in resistivity fit. The obtained α value from fitting is less than unity suggesting that at high-temperature thermoelectric transport is dominated by small polarons, the results are tabulated in Table 2.

Figure 8b shows the temperature-dependent power factor (*PF*) of pristine and EB-irradiated $Bi_{1.2}Pb_{0.33}Sr_{1.54}Ca_{2.06}Co_3O_y$, calculated using the formula $PF = S^2/\rho$. The PF value increases maximally as

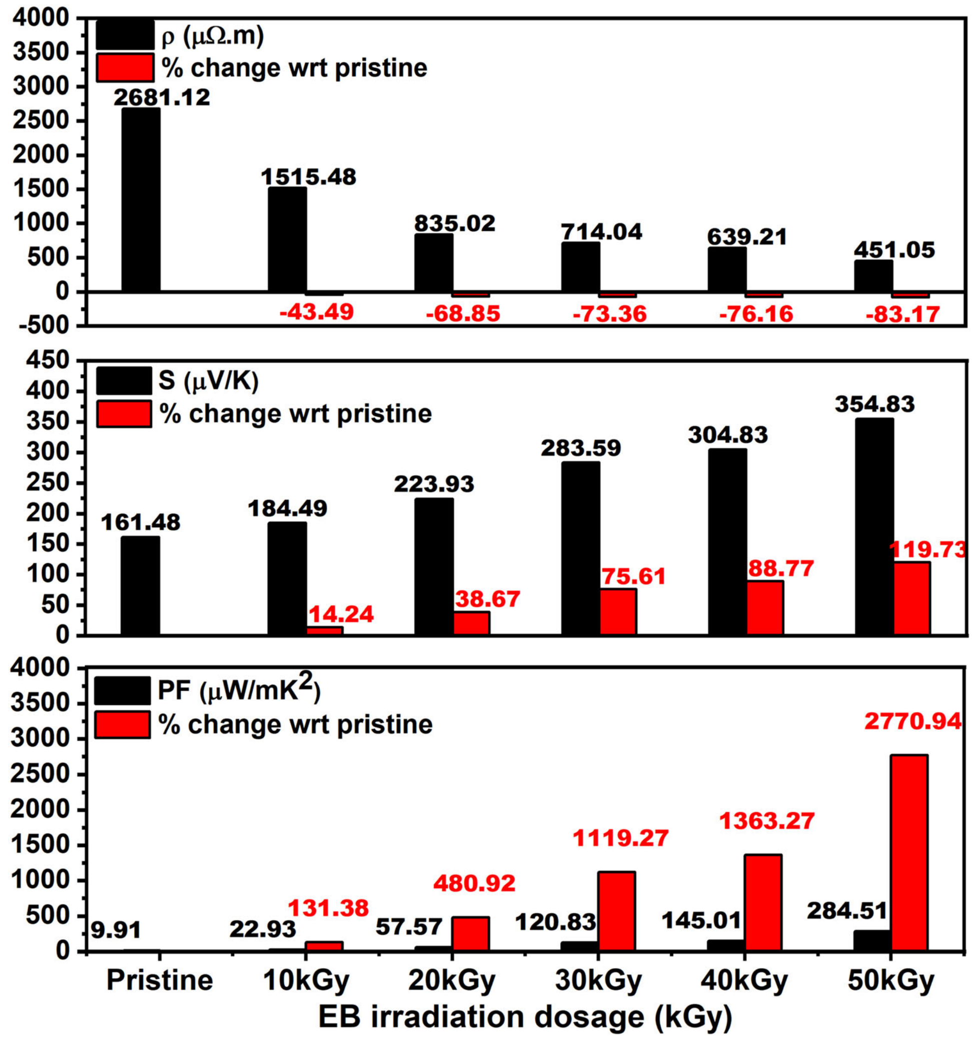

Fig. 9 Experimental values and percentage changes wrt pristine sample from the experimental data of pristine and EB-irradiated $Bi_{1.2}Pb_{0.33}Sr_{1.54}Ca_{2.06}Co_3O_y$ at 224 K

temperature rises and monotonically declines above 'Ts'. A similar pattern may be seen in the PF plot and the Seebeck coefficient plot. As discussed earlier, the b_1/b_2 ratio (misfitness) increases with increased EB irradiation, causing a decrease in electrical resistivity and an increase in the Seebeck coefficient, thereby resulting in an increase in the PF value. Our pristine non-stoichiometric sample shows a PF of $9.9\mu W/mK^2$ at 224K, which is higher than the previously reported PF in stoichiometric $Bi_{1.8}Pb_{0.2}Sr_2Ca_2Co_3O_x$ samples with a value of $\sim 1.25\mu W/mK^2$ at 224K [3], suggesting that non-stoichiometric compounds are more resilient and can show higher performance. The sample exposed to 50kGy of EB radiation possesses the maximum PF value, which is $\sim$ $284.51\mu W/mK^2$ at 224K. The increase/decrease percentage values of resistivity, Seebeck and PF with EB irradiation are shown in Fig. 9.

4 Conclusion

It is vital to increase the misfitness ratio (b1/b2) in thermoelectric cobalties to improve thermoelectric efficiency. A systematic study on the effect of electron beam irradiation on the thermoelectric properties of misfit $Bi_{1.2}Pb_{0.33}Sr_{1.54}Ca_{2.06}Co_3O_y$ has been carried out. It is evident from this study that the ratio of misfitness increased with an increase in EB dosage. SPH model and the data reveal that at high-temperature small polarons are accountable for conduction in pristine and EB-irradiated samples. The power factor is observed to increase with the increase in misfitness on exposing the samples to EB irradiation. The maximum power factor of $284.51\mu W/mK^2$ at 224K is evident in the 50kGy EB-irradiated sample. PF value increased by 2770.94% in the 50kGy EB-irradiated sample when compared to pristine $Bi_{1.2}Pb_{0.33}Sr_{1.54}Ca_{2.06}Co_3O_y$ at 224K. At the said temperature of 224K, this can be attributed to a decrease in electrical resistivity by 83.17% and an increase of the Seebeck coefficient by 119.73% in the 50kGy EB irradiated sample in comparison with the pristine sample.

Acknowledgements

This work is partially supported by financial grants from Science and Engineering Research Board-DST (EMR/2016/005424), New Delhi, India, and UGC-DAE- Consortium for Scientific Research, Indore centre (CSR-IC/CRS-89/2014- 2019) and its support as a user facility. SPR is indebted to the Maharaja Institute of Technology and Maharaja Research Foundation® (MRF) for a Research Fellowship and necessary support for the work via the Shodhana Research Scheme. We gratefully acknowledge eminent scientists and engineers; Dr Mukul Gupta and Layanta Behera for XRD; Dr Rajeev Rawat and Mr Sachin Kumar (MTC lab) for electrical measurements, Dr V. G. Sathe and Mr Ajay Rathore for Raman spectroscopy, Dr. D M Phase and Vinay K Ahire for SEM and EDS at UGC-DAE Consortium for Scientific Research, Indore.

Author contributions

SPR has been involved in the visualization, conceptualization, experiments, and drafting of the manuscript. AKS was involved in experimentation. CC, VPV, VCP, JD, and GO facilitated the experiments. VD has been engaged in visualization conceptualization, experiments, and writing (reviewing and editing) to improve the overall quality of the manuscript, supervision, and project administration.

Funding

This work is partially supported by Science and Engineering Research Board (IN), EMR/2016/005424, Vijaylakshmi Dayal.

Data availability

Data will be made available on reasonable request.

Declarations

Conflict of interests The authors declare that they have no known competing financial interests or personal relationships that could have appeared to influence the work reported in this paper.

References

1. E. Snyder, G.J. Toberer, Complex thermoelectric materials. Nat. Mater. **7**, 105–114 (2008). https://doi.org/10.1038/nmat2090
2. W. Di Liu, Z.G. Chen, J. Zou, Eco-friendly higher manganese silicide thermoelectric materials: progress and future challenges. Adv. Energy Mater. **8**, 1–18 (2018). https://doi.org/10.1002/aenm.201800056
3. A. Sotelo, E. Guilmeau, M.A. Madre, S. Marinel, J.C. Diez, M. Prevel, Fabrication and properties of textured Bi-based cobaltite thermoelectric rods by zone melting. J. Eur. Ceram. Soc. **27**, 3697–3700 (2007). https://doi.org/10.1016/j.jeurceramsoc.2007.02.020
4. Y. Kawaharada, K. Kurosaki, M. Uno, S. Yamanaka, Thermoelectric properties of CoSb3. J. Alloys Compd. **315**, 193–197 (2001). https://doi.org/10.1016/S0925-8388(00)01275-5
5. A.M. Ibrahim, D.A. Thompson, Thermoelectric properties of BiSb alloys. Mater. Chem. Phys. **12**, 29–36 (1985). https://doi.org/10.1016/0254-0584(85)90034-3
6. J. Yang, T. Aizawa, A. Yamamoto, T. Ohta, Thermoelectric properties of p-type (Bi2Te3)x(Sb2Te3)1–x prepared via bulk mechanical alloying and hot pressing. J. Alloys Compd. **309**, 225–228 (2000). https://doi.org/10.1016/S0925-8388(00)01063-X
7. H.Y. Lv, H.J. Liu, J. Shi, X.F. Tang, C. Uher, Optimized thermoelectric performance of Bi2Te3 nanowires. J. Mater. Chem. A. **1**, 6831–6838 (2013). https://doi.org/10.1039/c3ta10804j
8. C. Chang, M. Wu, D. He, Y. Pei, C.F. Wu, X. Wu, H. Yu, F. Zhu, K. Wang, Y. Chen, L. Huang, J.F. Li, J. He, L.D. Zhao, 3D charge and 2D phonon transports leading to high out-of-plane ZT in n-type SnSe crystals. Science **360**, 778–783 (2018). https://doi.org/10.1126/science.aaq1479
9. A. Nozariasbmarz, A. Agarwal, Z.A. Coutant, M.J. Hall, J. Liu, R. Liu, A. Malhotra, P. Norouzzadeh, M.C. Öztürk, V.P. Ramesh, Y. Sargolzaeiaval, F. Suarez, D. Vashaee, Thermoelectric silicides: A review. Jpn. J. Appl. Phys. (2017). https://doi.org/10.7567/JJAP.56.05DA04
10. Y. Li, G. Wang, M. Akbari-Saatlu, M. Procek, H.H. Radamson, Si and SiGe nanowire for micro-thermoelectric

generator: a review of the current state of the art. Front. Mater. **8**, 1–24 (2021). https://doi.org/10.3389/fmats.2021.611078
11. R. Funahashi, I. Matsubara, H. Ikuta, T. Takeuchi, U. Mizutani, S. Sodeoka, Oxide single crystal with high thermoelectric performance in air. Jpn. J. Appl. Phys. (2000). https://doi.org/10.1143/jjap.39.l1127
12. G.S. Nolas, J. Poon, M. Kanatzidis, Recent developments in bulk thermoelectric materials. MRS Bull. **31**, 199–205 (2006). https://doi.org/10.1557/mrs2006.45
13. H.J. Kim, H. Bin Bae, Y. Park, S.H. Choi, Defect-engineered Si1-xGex alloy under electron beam irradiation for thermoelectrics. Rsc Adv. **2**, 12670–12674 (2012). https://doi.org/10.1039/c2ra21567e
14. I. Terasaki, Y. Sasago, K. Uchinokura, Large thermoelectric power in single crystals. Phys. Rev. B **56**, R12685–R12687 (1997). https://doi.org/10.1103/PhysRevB.56.R12685
15. T. Takeuchi, T. Kondo, T. Takami, H. Takahashi, H. Ikuta, U. Mizutani, K. Soda, R. Funahashi, M. Shikano, M. Mikami, S. Tsuda, T. Yokoya, S. Shin, T. Muro, Contribution of electronic structure to the large thermoelectric power in layered cobalt oxides. Phys. Rev. B **69**, 1–9 (2004). https://doi.org/10.1103/PhysRevB.69.125410
16. T. Fujii, I. Terasaki, T. Watanabe, A. Matsuda, Large in-plane anisotropy on resistivity and thermopower in the misfit layered oxide Bi2-xPbxSr2Co2Oy. Japanese J Appl. Phys. Lett. **41**, 2–6 (2002). https://doi.org/10.1143/jjap.41.l783
17. R. Funahashi, I. Matsubara, H. Ikuta, T. Takeuchi, Thermoelectric properties of (Ca, Sr, $Bi)_2Co_2O_5$ whiskers. Mater. Trans. **42**, 956–960 (2001). https://doi.org/10.2320/matertrans.42.956
18. S. Hébert, D. Berthebaud, R. Daou, Y. Bréard, D. Pelloquin, E. Guilmeau, F. Gascoin, O. Lebedev, A. Maignan, Searching for new thermoelectric materials: Some examples among oxides, sulfides and selenides. J. Phys. Condens. Matter. (2016). https://doi.org/10.1088/0953-8984/28/1/013001
19. T. Fujii, I. Terasaki, The effects of the misfit structure on thermoelectric properties of Bi2-xPbxSr2Co2Oy Single crystals, Int. Conf. Thermoelectr. ICT, Proc. 2002-Janua (2002) 199–202. https://doi.org/10.1109/ICT.2002.1190299.
20. I. Terasaki, Cobalt oxides and Kondo semiconductors: A pseudogap system as a thermoelectric material. Mater. Trans. **42**, 951–955 (2001). https://doi.org/10.2320/matertrans.42.951
21. G.D. Mahan, J.O. Sofo, The best thermoelectric, Proc. Natl. Acad. Sci. U. S. A. 93 (1996) 7436–7439. https://doi.org/10.1073/pnas.93.15.7436.
22. A. Sotelo, G. Constantinescu, S. Rasekh, M.A. Torres, J.C. Diez, M.A. Madre, Improvement of thermoelectric properties of Ca 3Co 4O 9 using soft chemistry synthetic methods. J. Eur. Ceram. Soc. **32**, 2415–2422 (2012). https://doi.org/10.1016/j.jeurceramsoc.2012.02.012
23. K. Rubesova, T. Hlasek, V. Jakes, S. Huber, J. Hejtmanek, D. Sedmidubsky, Effect of a powder compaction process on the thermoelectric properties of Bi2Sr2Co1.8Ox ceramics. J. Eur. Ceram. Soc. **35**, 525–531 (2015). https://doi.org/10.1016/j.jeurceramsoc.2014.08.037
24. L.H. Yin, R. Ang, Y.N. Huang, H.B. Jiang, B.C. Zhao, X.B. Zhu, W.H. Song, Y.P. Sun, The contribution of narrow band and modulation of thermoelectric performance in doped layered cobaltites Bi 2 Sr 2 Co 2 O y. Appl. Phys. Lett. DOI (2013). https://doi.org/10.1063/1.4705429
25. L.H. Yin, R. Ang, Z.H. Huang, Y. Liu, S.G. Tan, Y.N. Huang, B.C. Zhao, W.H. Song, Y.P. Sun, Exotic reinforcement of thermoelectric power driven by Ca doping in layered Bi2Sr2 x Ca x Co2O y. Appl. Phys. Lett. (2013). https://doi.org/10.1063/1.4801644
26. A. Maignan, D. Pelloquin, S. Hebert, Y. Klein, M. Hervieu, Thermoelectric power in misfit cobaltites ceramics: optimization by chemical substitutions. Bol. La Soc. Esp. Ceram. y Vidr. **45**, 122–125 (2006). https://doi.org/10.3989/cyv.2006.v45.i3.290
27. Y. Tanaka, T. Fujii, M. Nakanishi, Y. Kusano, H. Hashimoto, Y. Ikeda, J. Takada, Systematic study on synthesis and structural, electrical transport and magnetic properties of Pb-substituted Bi-Ca-Co-O misfit-layer cobaltites. Solid State Commun. **141**, 122–126 (2007). https://doi.org/10.1016/j.ssc.2006.10.015
28. G. Constantinescu, S. Rasekh, M.A. Torres, J.C. Diez, M.A. Madre, A. Sotelo, Effect of Sr substitution for Ca on the Ca3Co4O 9 thermoelectric properties. J. Alloys Compd. **577**, 511–515 (2013). https://doi.org/10.1016/j.jallcom.2013.07.005
29. J.H. Markna, R.N. Parmar, D.G. Kuberkar, R. Kumar, D.S. Rana, S.K. Malik, Thickness dependent swift heavy ion irradiation effects on electronic transport of (La0.5 Pr0.2) Ba03 MnO 3 thin films. Appl. Phys. Lett. **88**, 10–13 (2006). https://doi.org/10.1063/1.2192087
30. A.B. Ravalia, M.V. Vagadia, P.G. Trivedi, P.S. Solanki, P.S. Vachhani, R.J. Choudhary, D.M. Phase, K. Asokan, N.A. Shah, D.G. Kuberkar, Modifications in device characteristics of La0.6Pr0.2Sr0.2MnO3/SrNb0.002Ti0.998O3 manganites by swift heavy ion irradiation. Indian J. Phys. **89**, 137–142 (2015). https://doi.org/10.1007/s12648-014-0524-4
31. B. Christopher, A. Rao, G.S. Okram, V. Chandra Petwal, V.P. Verma, J. Dwivedi, Comprehensive study on effect of electron beam irradiation on electrical, thermo-electric and magnetic properties of oxygen rich LaMnO3.15compound. J. Alloys Compd. **703**, 216–224 (2017). https://doi.org/10.1016/j.jallcom.2017.01.229

32. B. Christopher, A. Rao, V.C. Petwal, V.P. Verma, J. Dwivedi, W.J. Lin, Y.K. Kuo, Influence of electron beam irradiation on electrical, structural, magnetic and thermal properties of Pr0.8Sr0.2MnO3 manganites. Phys. B Condens. Matter. **502**, 119–131 (2016). https://doi.org/10.1016/j.physb.2016.08.053
33. S. Keshri, V. Dayal, S. Ravi, P.K. Nayak, AC susceptibility study in the single-phase Bi-2223 system. Czechoslov. J. Phys. **55**, 73–84 (2005). https://doi.org/10.1007/s10582-005-0009-y
34. A. Soni, G.S. Okram, Resistivity and thermopower measurement setups in the temperature range of 5–325 K. Rev. Sci. Instrum. **79**, 1–4 (2008). https://doi.org/10.1063/1.3048545
35. M. Tarachand, B. Saxena, G.S. Mukherjee, Okram, A load-based thermopower measurement setup in the temperature range of 5–330 K. Rev. Sci. Instrum. (2019). https://doi.org/10.1063/1.5090954
36. R.A. Young, The rietveld method. Zeitschrift Für Krist. - Cryst. Mater. **210**, 643–643 (1995). https://doi.org/10.1524/zkri.1995.210.8.643a
37. C. Frontera, J. Rodríguez-Carvajal, FullProf as a new tool for flipping ratio analysis. Phys. B Condens. Matter. **335**, 219–222 (2003). https://doi.org/10.1016/S0921-4526(03)00241-2
38. T. Fujii, I. Terasaki, T. Watanabe, A. Matsuda, Large in-plane anisotropy on resistivity and thermopower in the misfit layered oxide Bi2-xPbxSr2Co2Oy. Japanese J. Appl. Physics (2002). https://doi.org/10.1143/jjap.41.l783
39. X.G. Luo, Y.C. Jing, H. Chen, X.H. Chen, Intergrowth and thermoelectric properties in the Bi-Ca-Co-O system. J. Cryst. Growth. **308**, 309–313 (2007). https://doi.org/10.1016/j.jcrysgro.2007.07.037
40. G.K. Williamson, W.H. Hall, X-Ray broadening from filed aluminium and tungsten. Acta Metall. **1**, 22–31 (1953). https://doi.org/10.1016/0001-6160(53)90006-6
41. V. Mote, Y. Purushotham, B. Dole, Williamson-Hall analysis in estimation of lattice strain in nanometer-sized ZnO particles. J. Theor. Appl. Phys. (2012). https://doi.org/10.1186/2251-7235-6-6
42. P. Scherrer, Bestimmung der inneren Struktur und der Größe von Kolloidteilchen mittels Röntgenstrahlen. Kolloidchem. Ein Lehrb. **277**, 387–409 (1912). https://doi.org/10.1007/978-3-662-33915-2_7
43. D. Kim, G. Lee, O. Kim, prepared by sputtering Structural, optical, and transport properties of nanocrystalline bismuth telluride thin fi lms treated with homogeneous electron beam irradiation and thermal annealing. Nanotechnology **27**, 1–7 (2016). https://doi.org/10.1088/0957-4484/27/33/335703
44. S. Kudo, S. Tanaka, K. Miyazaki, Y. Nishi, M. Takashiri, Anisotropic analysis of nanocrystalline bismuth telluride thin films treated by homogeneous electron beam irradiation. Mater. Trans. **58**, 513–519 (2017). https://doi.org/10.2320/matertrans.M2016295
45. P. Chettri, U. Deka, A. Rao, K.K. Nagaraja, G.S. Okram, V.C. Petwal, V.P. Verma, J. Dwivedi, Effect of high energy electron beam irradiation on the structural properties, electrical resistivity and thermopower of La0.5Sr0.5MnO3 manganites. Phys. B Condens. Matter. **585**, 412119 (2020). https://doi.org/10.1016/j.physb.2020.412119
46. M.C. Weber, J. Kreisel, P.A. Thomas, M. Newton, K. Sardar, R.I. Walton, Phonon Raman scattering of RCrO 3 perovskites (R=Y, La, Pr, Sm, Gd, Dy, Ho, Yb, Lu). Phys. Rev. B. **85**, 1–9 (2012). https://doi.org/10.1103/PhysRevB.85.054303
47. M. An, S.K. Yuan, Y. Wu, Q.M. Zhang, X.G. Luo, X.H. Chen, Raman spectra of a misfit layered Ca3 Co4 O9 single crystal. Phys. Rev. B **76**, 1–5 (2007). https://doi.org/10.1103/PhysRevB.76.024305
48. S.K. Yuan, M. An, Y. Wu, Q.M. Zhang, X.G. Luo, X.H. Chen, Raman-scattering study of misfit-layered (Bi, Pb)-Sr-Co-O single crystal. J. Appl. Phys. **101**, 2–6 (2007). https://doi.org/10.1063/1.2745269
49. Y. Huang, B. Zhao, S. Lin, Y. Sun, Enhanced thermoelectric performance induced by misplaced substitution in layered Ca 3 Co 4 O 9. J. Phys. Chem. C (2015). https://doi.org/10.1021/jp512012d
50. V.G. Hadjiev, M.N. Iliev, I.V. Vergilov, The Raman spectra of Co3O4. J. Phys. C Solid State Phys. **21**, L199–L201 (1988). https://doi.org/10.1088/0022-3719/21/7/007
51. P. Lemmens, P. Scheib, Y. Krockenberger, L. Alff, F.C. Chou, C.T. Lin, H.U. Habermeier, B. Keimer, Comment on Raman spectroscopy study of Nax Co O2 and superconducting Nax Co O2 y H2O. Phys. Rev. B. (2007). https://doi.org/10.1103/PhysRevB.75.106501
52. H. Malekpour, P. Ramnani, S. Srinivasan, G. Balasubramanian, D.L. Nika, A. Mulchandani, R. Lake, A.A. Balandin, Thermal conductivity of suspended graphene with defects. Nanoscale (2016). https://doi.org/10.1039/c6nr03470e
53. B. Christopher, R. Thomas, A. Rao, G.S. Okram, V.C. Petwal, V.P. Verma, J. Dwivedi, A systematic study on effect of electron beam irradiation on electrical properties and thermopower of RE0.8Sr0.2CoO3 (RE=La, Pr) cobaltites. Phys. B Condens. Matter. **552**, 170–177 (2019). https://doi.org/10.1016/j.physb.2018.10.012
54. B. Christopher, A. Rao, U. Deka, S. Prasad K, G.S. Okram, G. Sanjeev, V. Chandraetwal, V.P. Verma, J. Dwivedi, Electrical, thermal and magnetic studies on 7.5 MeV electron beam irradiated PrCoO3 polycrystalline samples. Phys. B Condens. Matter. **540**, 26–32 (2018). https://doi.org/10.1016/j.physb.2018.04.026

55. C.J. Benedict, A. Rao, G. Sanjeev, G.S. Okram, P.D. Babu, A systematic study on the effect of electron beam irradiation on structural, electrical, thermo-electric power and magnetic property of LaCoO3. J. Magn. Magn. Mater. **397**, 145–151 (2016). https://doi.org/10.1016/j.jmmm.2015.08.111
56. B. R, Md Motin Seikh, V. Pralong, O.I. Lebedev, V. Caignaert, The ordered double perovskite PrBaCo2O6: Synthesis, structure, and magnetism. J. Appl. Phys. **114**, 1–5 (2013). https://doi.org/10.1063/1.4812368
57. E. Iguchi, K. Ueda, W.H. Jung, Conduction in LaCoO 3 by small-polaron hopping below room temperature. Phys. Rev. B. (1996). https://doi.org/10.1103/PhysRevB.54.17431
58. S.O. Manjunatha, A. Rao, T.Y. Lin, C.M. Chang, Y.K. Kuo, Effect of Ba substitution on structural, electrical and thermal properties of La0.65Ca0.35-xBaxMnO3($0 \leq x \leq 0.25$) manganites. J. Alloys Compd. **619**, 303–310 (2015). https://doi.org/10.1016/j.jallcom.2014.09.042
59. S.P. Rao, A.K. Saw, C. Chotia, G. Okram, V. Dayal, Structural and thermoelectric properties of Mn15Si26, Mn4Si7 and MnSi2, synthesized using arc-melting method. Appl. Phys. A Mater. Sci. Process. **127**, 1–6 (2021). https://doi.org/10.1007/s00339-021-04754-9

Publisher's Note Springer Nature remains neutral with regard to jurisdictional claims in published maps and institutional affiliations.